

## Self-consistent Simulation of Torque Generation by Radial Current due to Fast Particles

M. Honda 1), T. Takizuka 1), A. Fukuyama 2), M. Yoshida 1), T. Ozeki 1)

1) Japan Atomic Energy Agency, Naka, Ibaraki, Japan

2) Graduate School of Engineering, Kyoto University, Sakyo-ku, Kyoto, Japan

e-mail contact of main author: honda.mitsuru@jaea.go.jp

**Abstract.** The generation of the toroidal rotation due to the radial current torque induced by the charge separation is studied by using one-dimensional multi-fluid transport code TASK/TX. Taking account of the effect of the drift orbit, the charge separation occurs as long as trapped ions are generated, typically by near-perpendicular NBI. Coupling the TASK/TX code with the Orbit-Following Monte Carlo code OFMC, we have reproduced the toroidal rotation driven by the radial current by the near-perpendicular NBI with varying its vertical injection (poloidal) angle and clarified that the horizontal NBI drives the toroidal rotation most efficiently. By utilizing the radial current torque, we have elucidated that in a steady state the toroidal rotation is determined by the balance among the torque, the viscosity, the friction with neutrals and the loss of momentum due to charge exchange.

### 1. Introduction

Toroidal rotation and its shear play an important role in transport and stability of burning plasmas as well as the plasmas observed in present tokamak experiments. In current devices the rotation is easily driven and controlled by tangentially-injected neutral beam (NB) through a collisional slowing-down momentum transfer process. However, it is now commonly believed that the fast rotation is not expected in International Thermonuclear Experimental Reactor (ITER) because a self-generated alpha particle heating will be dominant and external heating systems may not be necessary. In addition, the collisional momentum transfer by tangential NBs would not be so large around the plasma core in an ITER plasma. There are a few reasons why so. First, the beam energy  $E_b$  is higher than that used in present devices and then the momentum input expressed by  $\sim P_b / \sqrt{E_b}$  becomes smaller, where  $P_b$  denotes the beam power. Second, because of the high density of the plasma, the mean free path of beam ions is short. Therefore they are likely to be trapped outboard of the plasma and are not deposited in the central region; this leads to a decrease in passing particles transferring their momentum to the bulk plasma.

Even in present tokamaks, trapped fast particles are favorably generated by perpendicular NB (PERP-NB) units. Several ‘‘near’’ PERP-NBs, whose typical injection angle to the field line on the magnetic axis is  $75^\circ$ , have been installed in JT-60U and the ions generated by them usually have a small parallel component of the velocity. In Fig. 1, we show an example of an orbit-following calculation during a first bounce period without the effect of the radial electric field  $E_r$  in JT-60U #45074 with the co PERP-NB. The effect of a toroidal field (TF) ripple is neglected in this calculation because the plasma is settled on the inboard side of the vacuum vessel, where the TF ripple is relatively weak. Most of the particles are toroidally trapped in the low-field side (LFS) of the plasma (Fig. 1 (a)). The remaining ions in the high-field side (HFS) of the plasma circulate around the torus (Fig. 1 (b)). In this case the collisional torque to the plasma is small. However, the trapped particles can also transfer their momentum to the bulk plasma in a different way. The mechanism is rather complicated than that in the case of passing particles because to the lowest order in gyroradius banana particles do not carry angular momentum: Their collisional torque to the plasma is canceled out during a bounce motion. When we consider a finite orbit effect due to a drift motion, the electron almost stays on the flux surface where the beam neutral is ionized, while the ion moves radially inward or outward depending on the injection direction, co- or counter-current. This instantaneous charge separation produces a fast-ion radial current  $j_f$  and it generates a return current  $j_{\text{bulk}}$  in the bulk

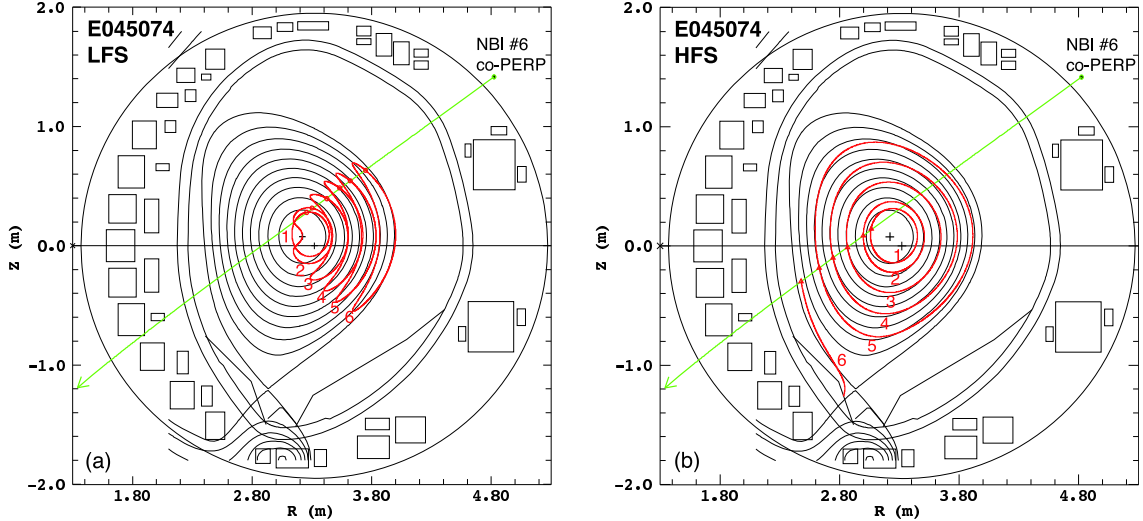


FIG. 1. Collisionless ion orbits generated by co near-perpendicular NBI #6 in JT-60U #45074. Each ion orbit is labeled by a number and the same number in both figures means that the ion is deposited on the same flux surface along the NBI. In the case that ions are deposited in LFS shown in (a), the ion nearest the magnetic axis becomes passing one (1), and the ion adjacent to (1) draws a potato orbit (2). All the other ions labeled by 3 to 6 draw banana orbits and their banana widths do not make much difference among them. In the case of HFS shown in (b), all the ions draw passing orbits except one labeled by 6, which is immediately lost from the plasma due to a collision with a divertor.

plasma, which exerts a  $j_{\text{bulk}} \times B$  torque [1]. As noted in Ref. [1], the rate of toroidal momentum input to the plasma, from either trapped or untrapped fast ions, is equal to the incident toroidal momentum input rate from the beam, in the light of momentum conservation. This implies that the  $j_{\text{bulk}} \times B$  torque, which is mainly generated by trapped particles, is not negligible for the correct evaluation of the total momentum input from NBIs. Therefore a quantitative evaluation of the  $j_{\text{bulk}} \times B$  torque is indispensable to predictions of the toroidal rotation in present devices as well as ITER.

The  $j_{\text{bulk}} \times B$  torque has been evaluated numerically by using Monte Carlo codes [2, 3] and analytically by solving the Fokker-Planck equation [4]. For a self-consistent understanding of the rotation induced by the radial current, however, simultaneous consideration of poloidal and toroidal rotations with the  $E_r$  effect, which has not been carried out so far, is indispensable through self-consistent transport simulations [5]. In this paper, an ideal concentric plasma equilibrium comparable in size to JT-60U is assumed to eliminate geometrical effects on and grasp the underlying physics associated with the torque. The torque generated by the charge separation and the resultant toroidal rotation are then comprehensively studied by using a multi-fluid transport code TASK/TX [6] cooperating with an orbit-following Monte Carlo code OFMC [7], and roles of the torque input against plasma profiles are examined to assess rotation control techniques in plasmas.

## 2. One-dimensional Multi-fluid Transport Code, TASK/TX

We outline the main features of the one-dimensional multi-fluid transport code TASK/TX [6] in the following with particular emphasis on the difference from conventional transport codes: (1) The code solves the continuity equations, the thermal transport equations and the two-fluid equations of motion for electrons and ions coupled with Maxwell's equations as well as the equations for neutrals and fast beam ions in the cylindrical coordinates  $(r, \theta, \phi)$ , where  $r, \theta$  and  $\phi$  denote the radial, poloidal and toroidal coordinates respectively. (2) Solving both the continuity equations for all charged particle species and Poisson's equation requires no explicit quasi-

neutrality condition. (3) The neoclassical effects such as the bootstrap current and the Ware pinch are originated from the parallel viscous force term in the poloidal equation of motion. (4) Turbulent ambipolar transport is expressed by the poloidal momentum exchange between electrons and ions; hence an explicit particle diffusion term is not necessary in the continuity equations. (5) The code takes account of the transport in the scrape off layer (SOL) in order to investigate a structure of a plasma near the plasma surface (separatrix). (6) The formation of  $E_r$  is evaluated consistent with the flows.

The feature (2) is important for this study because the difference in the orbit width of electrons and beam ions is treated as the difference in the shape of their birth profiles in the code.

In the following we briefly describe the main equations. The time evolution of the plasma is described by flux-surface averaged quantities for species  $s$ : the density  $n_s$ , the radial, poloidal and toroidal flow velocities  $u_{sr}$ ,  $u_{s\theta}$ ,  $u_{s\phi}$ , and the internal energy  $3/2n_sT_s$ . The equations are

$$\frac{\partial n_s}{\partial t} = -\frac{1}{r} \frac{\partial}{\partial r} (r n_s u_{sr}) + S_s, \quad (1)$$

$$\frac{\partial}{\partial t} (m_s n_s u_{sr}) = -\frac{1}{r} \frac{\partial}{\partial r} (r u_{sr} m_s n_s u_{sr}) + \frac{1}{r} m_s n_s u_{s\theta}^2 + e_s n_s (E_r + u_{s\theta} B_\phi - u_{s\phi} B_\theta) - \frac{\partial}{\partial r} (n_s T_s), \quad (2)$$

$$\begin{aligned} \frac{\partial}{\partial t} (m_s n_s u_{s\theta}) &= -\frac{1}{r^2} \frac{\partial}{\partial r} (r^2 u_{sr} m_s n_s u_{s\theta}) + \frac{1}{r^2} \frac{\partial}{\partial r} \left[ r^3 m_s n_s \mu_s \frac{\partial}{\partial r} \left( \frac{u_{s\theta}}{r} \right) \right] + e_s n_s (E_\theta - u_{sr} B_\phi) \\ &+ F_{s\theta}^{\text{NC}} + F_{s\theta}^{\text{C}} + F_{s\theta}^{\text{W}} + F_{s\theta}^{\text{L}} + F_{s\theta}^{\text{N}} + F_{s\theta}^{\text{CX}}, \end{aligned} \quad (3)$$

$$\begin{aligned} \frac{\partial}{\partial t} (m_s n_s u_{s\phi}) &= -\frac{1}{r} \frac{\partial}{\partial r} (r u_{sr} m_s n_s u_{s\phi}) + \frac{1}{r} \frac{\partial}{\partial r} \left( r m_s n_s \mu_s \frac{\partial u_{s\phi}}{\partial r} \right) + e_s n_s (E_\phi + u_{sr} B_\theta) \\ &+ F_{s\phi}^{\text{C}} + F_{s\phi}^{\text{W}} + F_{s\phi}^{\text{L}} + F_{s\phi}^{\text{N}} + F_{s\phi}^{\text{CX}}, \end{aligned} \quad (4)$$

$$\begin{aligned} \frac{\partial}{\partial t} \left( \frac{3}{2} n_s T_s \right) &= -\frac{1}{r} \frac{\partial}{\partial r} \left( \frac{5}{2} r u_{sr} n_s T_s \right) + \frac{1}{r} \frac{\partial}{\partial r} \left( r n_s \chi_s \frac{\partial T_s}{\partial r} \right) + u_{sr} \frac{\partial}{\partial r} n_s T_s + e_s n_s (E_\theta u_{s\theta} + E_\phi u_{s\phi}) \\ &+ P_s^{\text{C}} + P_s^{\text{B}} + P_s^{\text{L}} + P_s^{\text{R}} + P_s^{\text{RF}}, \end{aligned} \quad (5)$$

where  $m_s$  and  $e_s$  are the mass and charge respectively. The perpendicular viscosity  $\mu_s$  and thermal conductivity  $\chi_s$  represent anomalous transport contributions due to turbulent fluctuations. Here the particle source denotes  $S_s$ , neoclassical viscous force  $F_s^{\text{NC}}$ , classical collisional momentum transfer force  $F_s^{\text{C}}$  between different species including beam ions, forces due to the wave-particle interaction  $F_s^{\text{W}}$ , parallel transport loss in the SOL region  $F_s^{\text{L}}$ , friction force with neutrals  $F_s^{\text{N}}$ , charge exchange force  $F_s^{\text{CX}}$ , collisional energy transfer power  $P_s^{\text{C}}$ , heating power from NBIs  $P_s^{\text{B}}$ , collisional energy loss power in the SOL  $P_s^{\text{L}}$ , bremsstrahlung loss power  $P_s^{\text{R}}$  and direct RF heating power  $P_s^{\text{RF}}$ .

Maxwell's equations are simultaneously solved for the evolution of the electromagnetic fields, that is, the radial, poloidal and toroidal electric fields  $E_r$ ,  $E_\theta$ , and  $E_\phi$ , and the poloidal and toroidal magnetic fields  $B_\theta$ ,  $B_\phi$  as follows:

$$\frac{1}{r} \frac{\partial}{\partial r} (r E_r) = \frac{1}{\epsilon_0} \sum_s e_s n_s, \quad (6)$$

$$\frac{1}{c^2} \frac{\partial E_\theta}{\partial t} = -\frac{\partial B_\phi}{\partial r} - \mu_0 \sum_s e_s n_s u_{s\theta}, \quad \frac{\partial B_\theta}{\partial t} = \frac{\partial E_\phi}{\partial r}, \quad (7)$$

$$\frac{1}{c^2} \frac{\partial E_\phi}{\partial t} = \frac{1}{r} \frac{\partial}{\partial r} (r B_\theta) - \mu_0 \sum_s e_s n_s u_{s\phi}, \quad \frac{\partial B_\phi}{\partial t} = -\frac{1}{r} \frac{\partial}{\partial r} (r E_\theta), \quad (8)$$

where  $\epsilon_0$  and  $\mu_0$  are the permittivity and the permeability in a vacuum respectively, and  $c$  is the speed of light.

The continuity equation and the slowing-down equations for beam ions are given by

$$\frac{\partial n_b}{\partial t} = S_b - \nu_b n_b - \nu_{bL} n_b, \quad (9)$$

$$\frac{\partial}{\partial t}(m_b n_b u_{b\theta}) = e_b n_b E_\theta + F_{b\theta}^C + F_{b\theta}^L + F_{b\theta}^N + F_{b\theta}^{CX} + F_{b\theta}^B - \nu_{bL} m_b n_b u_{b\theta}, \quad (10)$$

$$\frac{\partial}{\partial t}(m_b n_b u_{b\phi}) = e_b n_b E_\phi + F_{b\phi}^C + F_{b\phi}^L + F_{b\phi}^N + F_{b\phi}^{CX} + F_{b\phi}^B - \nu_{bL} m_b n_b u_{b\phi}, \quad (11)$$

where  $\nu_b$  denotes the slowing-down rate,  $\nu_{bL}$  the loss rate to the divertor in the SOL and  $F_{b\phi}^B$  the direct collisional torque input from NBIs. Although the code also contains the diffusion equations for two-group neutrals, we omit the description in this paper. More details about the code can be seen in Refs. [6, 8]

### 3. Charge Separation due to NBIs

Owing to the toroidal drift induced by the toroidicity of a tokamak, a drift surface does not coincide with a magnetic flux surface. A departure from the flux surface is typically given by  $\Delta_p \approx \varepsilon \rho_\theta$  for passing particles and  $\Delta_b \approx \sqrt{\varepsilon} \rho_\theta$  for trapped (banana) ones respectively, where  $\varepsilon$  is the inverse aspect ratio and  $\rho_\theta$  the poloidal Larmor radius. As clear from the above relations, the departure for banana particles is  $\sqrt{\varepsilon}$  times as much as that for passing ones. We then focus on the effect of the departure for trapped particles only in this study. Although these relations are valid for both electrons and ions, the departure for electrons are much smaller than that for ions because of  $\rho_\theta \propto \sqrt{m}$  and  $m_e \ll m_i$ . When fast ions and accompanying electrons are generated from beam neutrals on a flux surface, therefore, we reasonably assume that the electrons stay on the surface while the ions are deviated radially and then they reside on the different flux surfaces. This causes a steady charge separation as long as the NB is injected into the plasma. Compensating this local charge imbalance to maintain quasi-neutrality, a radial return current flows in the bulk plasma. Finally this current induces the  $j_{\text{bulk}} \times B$  torque, driving the toroidal rotation. This torque always drives the plasma in the direction of the NB injection. In this study, we only use a co PERP-NB so that we consider ‘‘well-confined’’ banana ions and neglect the intersection of the orbit with the wall during a first bounce motion.

In order to quantitatively evaluate a birth profile by the co PERP-NB including the finite orbit effect, we have upgraded the OFMC code. Using background profiles calculated by TASK/TX, OFMC distinctly calculates birth profiles for both trapped and passing ions as follows: After following orbits of 10,000 test particles during a first bounce motion, OFMC labels all the particles trapped or passing and then follows the orbits back to their creation, and evaluates their birth positions retroactively. For each particle, OFMC checks the flux surface on which the particle is located every minute time step, typically  $\sim \tau_b/100$  where  $\tau_b$  is the bounce time, until its orbit projected to the poloidal plane is closed. The time spent on each surface is renormalized by  $\tau_b$  to estimate the existing probability of the particle on each surface. OFMC iterates this procedure for all the test particles. Then it sums up the contributions of them and multiply the resultant distribution function by the number of actual particles injected into the plasma per second. We thus obtain NB source profiles at birth with the effect of the finite orbit width for both trapped and passing particles. As mentioned above, however, we take account of the orbit effect for banana particles only in this study.

### 4. Toroidal Torque Induced by Charge Separation

Owing to the features of the TASK/TX code described in Section 2, simply giving birth profiles for beam ions and electrons calculated by OFMC to the TASK/TX code allows us to

simulate a plasma evolution including the toroidal rotation driven by the charge separation. We use the plasma parameters similar to JT-60U #45074: the major radius  $R = 3.22$  m, the minor radius  $a = 0.8$  m, the toroidal magnetic field  $B_\phi = 2.68$  T, the plasma current  $I_p = 0.8$  MA and the safety factor at 95% flux surface  $q_{95} = 2.5$ . The concentric circular equilibrium is assumed for simplicity. We use particle and thermal diffusivities so as to roughly reproduce the steady-state profiles of the electron density and electron and ion temperatures observed in the experiment, and assume that the viscosity  $\mu_s$  is equal to the thermal diffusivity  $\chi_s$ :  $\mu_s = \chi_s$ .

The co PERP-NB of 2.37 MW with the mono-energy of 82 keV is injected with three different poloidal angles: (a)  $0^\circ$ , (b)  $30^\circ$  and (c)  $60^\circ$ . It is tilted from a fully perpendicular beam line so that a birth ion roughly has a pitch angle of  $75^\circ$  in case (a). As shown in Fig. 2, we find that the pitch angle of the birth ion is gradually changing as the poloidal angle increases because the shapes of the orbits differ from each other in spite of the generation on the same flux surface. When the orbits are compared between case (a) and (b), the overall tendency is almost the same for both trapped and passing ions in LFS and HFS of the torus, except for the slight difference in the banana width. The banana width is rather fat in case (a) and the shape of the orbit is similar to that of the potato orbit. On the other hand, the beam line (c) generates the trapped ion with relatively slim banana width in the LFS and also the barely trapped ion even in the HFS. This difference is ascribed to the magnitude of the magnetic field at the birth point. Focusing on a certain flux surface, the magnetic field at the birth point in the LFS is gradually increasing and that in the HFS is decreasing as a tilt of the beam line from the mid-plane is increasing. Under the constant energy and power of the NBI and conservation of the magnetic moment, the tip point where the parallel velocity is zero changes with the change in the field strength and then the shape of the orbit also changes.

Giving OFMC the density and temperature profiles by TASK/TX at  $t = 50$  ms after the initial phase, birth profiles of both trapped and passing ions and trapped ions with the banana width effect are exhibited in Fig. 3, calculated by OFMC. The birth of the passing ions is localized in  $\rho \equiv r/a \lesssim 0.2$ , i.e.  $\psi \lesssim 0.075$ , and no trapped ions are generated in the region as seen in Fig. 3 (a) and (b). The banana width effect is found to contribute to the inward shift of the trapped ion profile. Since the banana width becomes fatter as the birth point approaches the magnetic axis, the averaged position of the trapped ion moves inward compared to its birth point. We note that the reason that the peak is formed in the density profile of birth ions is that at the very near magnetic axis a volume surrounded by a flux surface is very small.

We carry out TASK/TX simulations for three cases (a), (b) and (c) by utilizing the birth profiles from OFMC. After 50 ms ohmic calculation the co PERP-NB is injected into the plasma with the line-averaged electron density  $\bar{n}_e = 1.37 \times 10^{19} \text{ m}^{-3}$  and temperature  $\bar{T}_e = 0.753$  keV, and the plasma is assumed to reach a steady state at  $t = 2$  s. Figure 4 (1) shows the profiles of  $E_r$  and the ion toroidal velocity  $u_{i\phi}$  with both the collisional and  $j_{\text{bulk}} \times B$  effects. The viscosity shown in Fig. 4 (3) below is given and fixed throughout the simulations. We see in Fig. 4 (1) the centrally-peaked toroidal rotation profiles corresponding to the centrally-peaked birth profiles of the passing ions. If we neglect the contribution of the collisional torque, we then obtain a

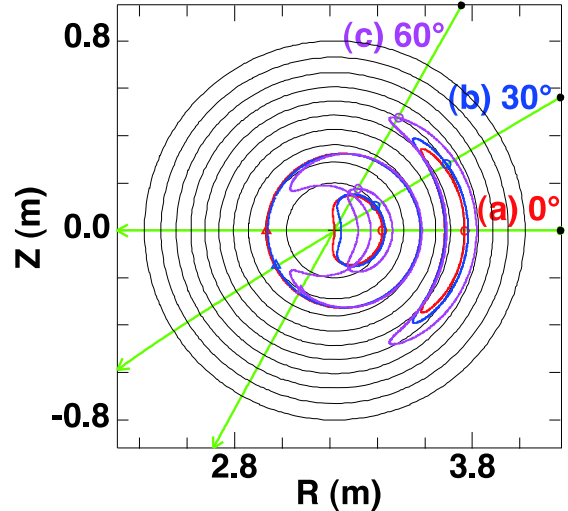


FIG. 2. Co PERP neutral beam lines with different poloidal angles of (a)  $0^\circ$ , (b)  $30^\circ$  and (c)  $60^\circ$  in a concentric cylindrical equilibrium. Typical orbits of beam ions at  $\psi = 0.1, 0.6$  of LFS and  $\psi = 0.2$  of HFS are drawn for each beam line, where  $\psi$  denotes the poloidal flux.

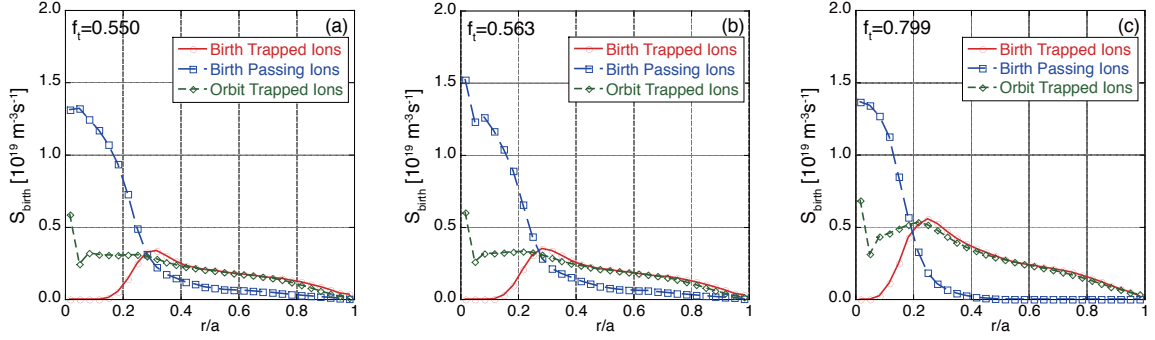


FIG. 3. Birth profiles of both trapped and passing ions and trapped ions with the banana width effect calculated by OFMC. The figures (a), (b) and (c) correspond to the beam lines shown in Fig. 2 and the corresponding shine-through powers are 0.96 MW, 0.94 MW and 0.97 MW, respectively. Here  $f_t$  denotes the fraction of the trapped particles.

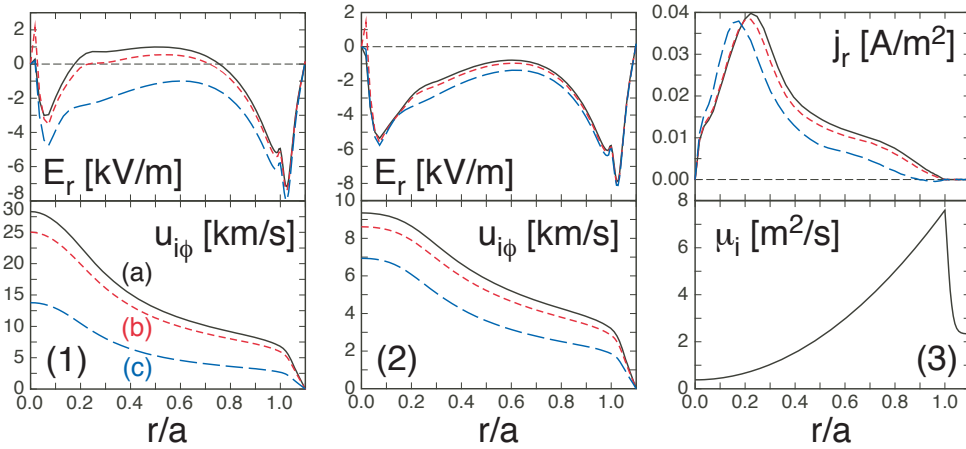


FIG. 4. The radial electric field  $E_r$  and the ion toroidal velocity  $u_{i\phi}$  at  $t = 2$  s in the cases (1) with both collisional and  $j_{\text{bulk}} \times B$  torques and (2) with  $j_{\text{bulk}} \times B$  torque only. The radial current  $j_r$  and the viscosity  $\mu_i$ , which is given and fixed throughout the simulations, are shown in (3). The colored indices (a), (b) and (c) correspond to the beam lines shown in Fig. 2, respectively.

broader and slower rotation profile in Fig. 4 (2), purely driven by the  $j_{\text{bulk}} \times B$  torque. When we compare the profile (c) with (a) and (b) in Fig. 4 (1), the rotation (c) is clearly smaller than the others. Considering the relatively small decrease in the  $j_{\text{bulk}} \times B$  torque found in Fig. 4 (2), we deduce that the reason is ascribed to the reduction in the collisional torque. Figure 2 shows that the co PERP-NB (c) generates the trapped ion even in the HFS as well as LFS. In addition, comparing three figures in Fig. 3 reveals that it produces more trapped ions and less passing ions. As a result, the decrease in both the number of the passing ions, directly driving the plasma rotation, and the  $j_{\text{bulk}} \times B$  torque leads to the decrease in  $u_{i\phi}$  labeled by (c).

Next we examine the reason of the decrease in the  $j_{\text{bulk}} \times B$  torque with the beam line tilted upward, i.e. from (a) to (c), as shown in Fig. 4 (2). To understand the mechanism, we focus on the radial current  $j_{\text{bulk}}$  generated in the bulk plasma shown in Fig. 4 (3) above. With increasing the angle from  $0^\circ$  to  $60^\circ$ , the current density profile seems to shift inward and locally decrease in  $\rho > 0.2$ . The decrease depends on where a birth position of an ion is on a flux surface. As can be seen in Fig. 2, the birth position in case (c) is very close to the banana tip in comparison with case (a) and (b), and the ion draws the banana orbit across the flux surface at birth: In a first half of a bounce motion it runs deeply inward from the birth surface and in the latter half it almost does outward. By averaging the deviation of the trapped ion from the birth surface over a bounce motion, the contribution of the inward deviation is to some extent offset by that of the outward one. Therefore the averaged inward deviation from the birth flux surface is

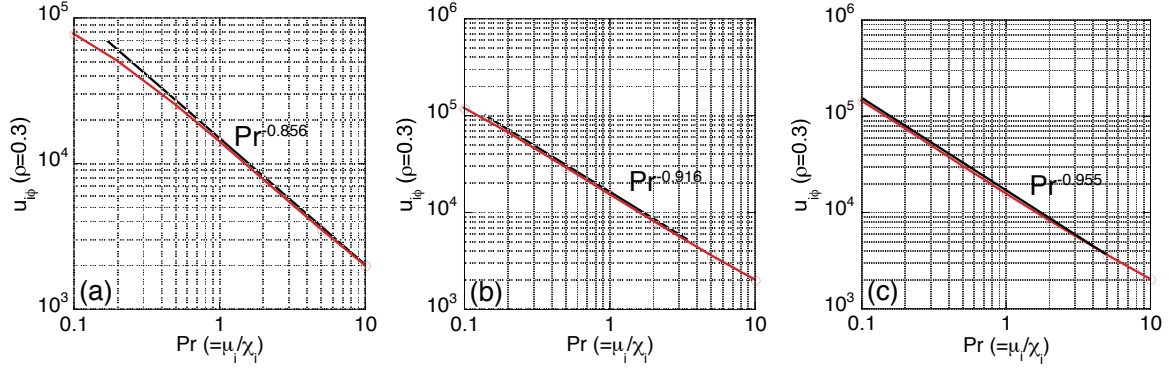


FIG. 5. Dependence of the toroidal rotation  $u_{i\phi}$  on the Prandtl number  $Pr$  in the case (a) with the full terms, (b) without the collision terms with neutrals and (c) without the collision terms with neutrals and the convection terms, in the equations of motion. The black lines are eye-guide ones.

relatively small, although the banana width is broader than the others, leading to the decrease in  $j_{\text{bulk}}$ . Since a volume surrounded by a flux surface is smaller in the inboard and larger in the outboard, the generated current and the resultant torque become smaller on the whole.

## 5. Relation between Steady-state Toroidal Rotation and the Prandtl Number

Even if an external torque is constantly injected into a plasma, it finally approaches a steady state and the toroidal rotation settles down at a certain value and profile. In a steady state, the presence of terms balancing the torque input is imperative and the possible candidate is widely believed to be a viscous term. If we assume that the rotation is determined by the balance between the torque and viscosity only, it is estimated from the second term of the left-hand side of Eq. (4) as  $u_{i\phi} = (L^2/\mu_i)F$ , where  $L$  is a characteristic length of the  $u_{i\phi}$  profile and  $F$  a torque. If  $F$  is kept constant and is independent on  $\mu_i$ ,  $u_{i\phi}$  is inversely proportional to  $\mu_i$ ,  $u_{i\phi} \propto \mu_i^{-1}$ . We then examine what regulates  $u_{i\phi}$  in a steady state under the condition of a constant torque input, by changing the viscosity. In the following we use the Prandtl number defined as the ratio of the viscosity to the thermal diffusivity,  $Pr \equiv \mu_i/\chi_i$ , instead of  $\mu_i$ .

The  $j_{\text{bulk}} \times B$  torque is suitable for a constant torque input into the plasma, because it instantaneously becomes constant compared with the collisional torque. In this study, we adopt the same plasma parameters used in the previous section. For simplicity, the collisional torque by a co PERP-NB is neglected and the banana orbit effect is analytically calculated as  $\Delta_b = \sqrt{\epsilon}\rho_\theta$ . We artificially increase 100 times as much the parallel loss to the divertor in the SOL as the standard case in order to eliminate the effect of the pedestal  $u_{i\phi}$  on the core one. We then carry out simulations with the  $j_{\text{bulk}} \times B$  torque input until the plasma reaches a steady state, changing the viscosity, and examine the dependence of  $u_{i\phi}$  at  $\rho = 0.3$ , which is chosen as a typical value in the core region, on  $Pr$ .

The simulation result shown in Fig. 5 (a) clearly reveals that  $u_{i\phi}$  is not in inverse proportion to  $Pr$ :  $u_{i\phi} \propto Pr^{-0.856}$ . Furthermore, the red line gradually deviates downward from the  $Pr^{-0.856}$  dependence as  $Pr$  decreases. It means that although the steady-state value of  $u_{i\phi}$  is mainly determined by  $\mu_i$ , other effects are not negligible. Particularly, the deviation from  $Pr^{-0.856}$  in the limit of the small viscosity indicates existence of a drag force: Since the rotation velocity increases with the decrease in the viscosity, we deduce that the above-mentioned force possibly relates to the momentum loss that increases proportionally with the velocity. Therefore we eliminate both the friction force with neutrals  $F_s^N$  and the loss of momentum due to charge exchange  $F_s^{\text{CX}}$  from the equations of motion, Eqs. (3), (4), (10) and (11). The result shown in Fig. 5 (b) shows a more inversely proportional dependence of  $u_{i\phi} \propto Pr^{-0.916}$  and an almost

constant gradient over the  $Pr$  space, nevertheless we can still find the slight deviation in  $Pr < 0.2$ . Although the convective momentum loss is smaller than other effects mentioned above, it may steadily carry the momentum out of the plasma and it is possibly capable of affecting the momentum balance. We then eliminate the convective terms and their related terms from the equations of motion, corresponding to the first and second terms in Eq. (2) and the first terms in Eqs. (3) and (4). This elimination further improves the inverse linearity between  $u_{i\phi}$  and  $Pr$ :  $u_{i\phi} \propto Pr^{-0.955}$  as shown in Fig. 5 (c). In addition, the dependence  $u_{i\phi} \propto Pr^{-0.955}$  holds over the  $Pr$  space even in the limit of the small viscosity. We note that we have confirmed that other factors appearing our model equations hardly affect the relation between  $u_{i\phi}$  and  $Pr$ .

## 6. Conclusions

We have studied the toroidal rotation induced by the torque due to the charge separation by the co-PERP NB, utilizing the TASK/TX code. Coupling TASK/TX with OFMC, self-consistent simulations have reproduced the generation of the toroidal rotation arising from the  $j_{\text{bulk}} \times B$  torque. Although the toroidal angle of the co PERP-NB is fixed, the birth profiles for both trapped and passing ions varies as the poloidal angle of the beam line increases. This is because the trapped particle fraction and the birth position on the banana orbit change according to the angle. In the cases that the beam line passes through the magnetic axis, the TASK/TX simulations have clarified that the horizontally-injected NB drives the plasma rotation most efficiently with respect to both collisional and  $j_{\text{bulk}} \times B$  torques and that the amplitude of the latter torque is not simply proportional to the banana width.

From the simulations with varying the Prandtl number, the following facts are clarified: Within the system of the present TASK/TX code, the toroidal velocity is mainly regulated by the balance between the external torque and the viscosity. However, the momentum loss processes due to convection and collisions with neutrals through the friction and the charge exchange also play a important role in predicting the toroidal rotation velocity.

This work was supported by the Grant-in-Aid for Young Scientists (Start-up) from Japan Society for the Promotion of Science (JSPS).

## References

- [1] HINTON, F.L., ROSENBLUTH, M.N., “The mechanism for toroidal momentum input to Tokamak plasmas from neutral beams”, *Phys. Lett. A* **259** (1999) 267.
- [2] SUCKEWER, S., et al., “Toroidal Plasma Rotation in the Princeton Large Torus Induced by Neutral-Beam Injection”, *Phys. Rev. Lett.* **43** (1979) 207.
- [3] HELANDER, P., AKERS, R.J., “On neutral-beam injection counter to the plasma current”, *Phys. Plasmas* **12** (2005) 112503.
- [4] ZASTROW, K.-D., et al., “TRANSFER RATES OF TOROIDAL ANGULAR MOMENTUM DURING NEUTRAL BEAM INJECTION”, *Nucl. Fusion* **38** (1998) 257.
- [5] CHANG, C.S., “Plasma rotation under a driven radial current in a tokamak”, *Nucl. Fusion* **39** (1999) 2113.
- [6] HONDA, M., FUKUYAMA, A., “Dynamic transport simulation code including plasma rotation and radial electric field”, *J. Comp. Phys.* **227** (2008) 2808.
- [7] TANI, K., et al., “Effect of Toroidal Field Ripple on Fast Ion Behavior in a Tokamak”, *J. Phys. Soc. Jpn.* **50** (1981) 1726.
- [8] HONDA, M., et al., “Numerical analysis of the effect of fast-ion losses on plasma rotation in a tokamak with toroidal field ripple”, *Nucl. Fusion* **48** (2008) 085003.